

# <sup>1</sup> Chapter 1

## <sup>2</sup> Diamond irradiation study

<sup>3</sup> The aim of the study in this chapter is to find the operational limitations of diamond  
<sup>4</sup> detectors for spectroscopy and tracking applications. The chapter contains the measurement  
<sup>5</sup> results of data taken with diamond sensors. First the measurement setup is described in  
<sup>6</sup> section 1.1. Then the measured particle spectra are shown in 1.2. This is followed by a  
<sup>7</sup> study of effects of the irradiation damage on the electrical signal of the diamond detector.  
<sup>8</sup> The last section shows the results of the measurements of irradiated diamond samples at  
<sup>9</sup> cryogenic temperatures. The studies compare the experimentally acquired data with the  
<sup>10</sup> theory from the previous chapter and define limitations of the diamond detectors in terms  
<sup>11</sup> of radiation and temperature.

<sup>12</sup> Diamond sensors are mainly used for two types of measurements: particle counting and  
<sup>13</sup> spectroscopy. The first type of measurements depends on the sensor efficiency – its ability to  
<sup>14</sup> detect all or at least a known percentage of incident particles. The energy of the particles  
<sup>15</sup> is not so important; what bears the information is the rate and the spatial distribution.  
<sup>16</sup> Here the particles do not necessarily stop in the bulk, but rather continue their way. In  
<sup>17</sup> spectroscopy, on the other hand, the particles stop within the sensor, depositing all their  
<sup>18</sup> energy. This energy is then measured by collecting the freed charge carriers. The goal of  
<sup>19</sup> the experiments described in this chapter is to:

- <sup>20</sup> 1. Quantify the efficiency of the sCVD diamond in counting mode,
- <sup>21</sup> 2. Quantify the degradation of the efficiency as a function of the received radiation dose,
- <sup>22</sup> 3. Quantify the macroscopic effects on charge carrier behaviour as a function of the  
received radiation dose and
- <sup>23</sup> 4. Define limitations for use in spectroscopy.

<sup>25</sup> The results discussed here show that there are several limitations for using diamond as  
<sup>26</sup> a radiation detector. All of them need to be taken into account when designing a new  
<sup>27</sup> measurement device. The irradiation study allows for an estimation of the lifetime of the  
<sup>28</sup> detector and a prediction of the longterm signal degradation as a function of the received  
<sup>29</sup> radiation dose. The result of the study is a correction factor, which can be applied during  
<sup>30</sup> data analysis to ensure that the analysis results are stable despite the detector degradation.

## **1.1. MEASUREMENT SETUP**

---

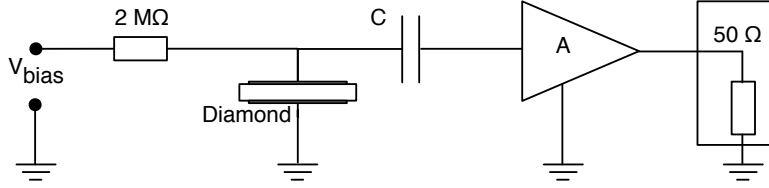


Figure 1.1: Diagram of a diamond detector readout chain.

### **31 1.1 Measurement setup**

32 The first step of designing a measurement setup is to define the measurement conditions,  
33 such as the temperature, the type of radiation and its flux. The second step is to ensure  
34 that the setup is insensitive to external electromagnetic interferences and that it minimises  
35 electrical noise in the system. The setup needs to be calibrated before use.

36 Shielding has to be applied wherever possible. For instance, aluminium foil can be  
37 wrapped around the exposed parts of the system to shield them from external radio-  
38 frequency (RF) interferences. In addition, the sensors have to be covered to prevent the  
39 exposure to light. The incident photons may deposit enough energy to increase the leakage  
40 current of the detector, which produces unwanted results.

41 The measurements using diamond that are explained in these chapters have been carried  
42 out using several measurement setups, but they are all similar in terms of the electrical  
43 signal chain. The measurement chain consists of three main parts: a diamond sensor, a  
44 signal preamplifier and a readout device, as seen in figure 1.1. The signals propagating  
45 along the analogue chain are fast – in the GHz bandwidth range – and with low amplitudes  
46 – of the order of tens of  $\mu\text{V}$ . This gives rise to the importance of RF shielding. Also, the  
47 connection between the carrier and the preamplifier has to be as short as possible to avoid  
48 capacitive signal losses in the transmission line. Finally, the system needs to be grounded  
49 properly.

#### **50 1.1.1 Preamplifiers**

51 Two preamplifiers are used for the measurements, one sensitive to charge and the other  
52 to current. *CIVIDEC Cx* (figure 1.2a) is a charge sensitive amplifier. Its high SNR is  
53 achieved due to a low equivalent noise charge of  $300 \text{ e}^-$  with an additional  $30 \text{ e}^-$  per each  
54 pF of the sensor capacitance. A reported gain of  $\sim 12 \text{ mV/fC}$  makes it a good choice for  
55 spectroscopic measurements with diamond sensors. *CIVIDEC C2* (figure 1.2b) is a fast  
56 current preamplifier with a 2 GHz bandwidth limit. It is used for TCT measurements  
57 because of its fast response and a good SNR. Both are embedded in an RF-tight aluminium  
58 box to reduce the noise pickup. Both have an AC coupled input and an output with a  $50 \Omega$   
59 termination.

60 A 2 GHz bandwidth limit defines the minimum rising time equal to  $t_r \simeq \frac{0.34}{BW} = \frac{0.34}{2 \times 10^9} =$   
61 170 ps, therefore the system with a CIVIDEC C2 amplifier is capable of measuring pulses

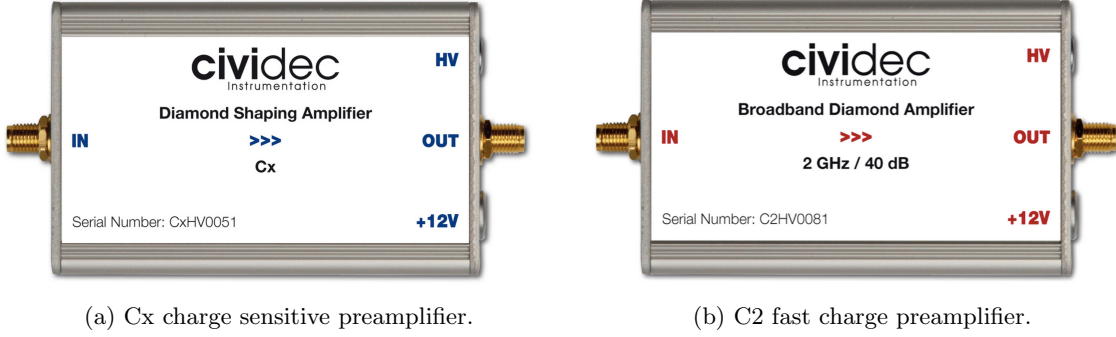


Figure 1.2: Amplifiers used for the charge and current measurements.

with a minimum  $\text{FWHM} \simeq 170 \text{ ps}$ . The initial peak in the  $\alpha$  pulse has a lower FWHM; for example, if a charge carrier travelling through the bulk takes  $t_1 \sim 6 \text{ ns}$  to reach the electrode on the opposite side ( $d_1 \sim 500 \mu\text{m}$ ), the carrier with the opposite charge and a shorter path to the closer electrode – max.  $d_2 \sim 10 \mu\text{m}$  – only takes  $t_2 \sim \frac{d_2}{d_1} t_1 = 120 \text{ ps}$ . A drift time this short induces a current pulse that is too narrow for the system to observe.

## Calibration

The amplifiers have to be calibrated before use to determine their gain. Both are calibrated using a square signal generator with a known amplitude step of  $U_{\text{in}} = (252 \pm 5) \text{ mV}$ . A 2 GHz oscilloscope with a 10 GS/s sampling rate is used to carry out the calibration.

**Cx charge sensitive amplifier** calibration necessitates an injection of a well known charge. Therefore the signal from a pulse generator is routed through a capacitor with a calibration capacitance  $C_{\text{cal}} = (0.717 \pm 0.014) \text{ pF}$  and then to the input of the amplifier. The pulse area behind the capacitor is  $a_{\text{cal}} = (5.0 \pm 0.5) \text{ pVs}$ , with the signal amplitude on the output amounting to  $U_{\text{Cx}} = (1.95 \pm 0.05) \text{ V}$ . The input voltage step combined with the calibration capacitance yields a calibration charge

$$Q_{\text{cal}} = C_{\text{cal}} \cdot U_{\text{in}} = (181 \pm 5) \text{ fC}. \quad (1.1)$$

The gain of the Cx amplifier when comparing the integrated input charge to the output amplitude is

$$A_{\text{Cx}}^Q = \frac{U_{\text{Cx}}}{Q_{\text{cal}}} = (9.3 \pm 0.4) \text{ mV/fC} \quad (1.2)$$

whereas the factor between the area of the input current pulse and the output amplitude is

$$A_{\text{Cx}}^a = \frac{U_{\text{Cx}}}{a_{\text{cal}}} = (390 \pm 40) \text{ mV/pVs}. \quad (1.3)$$

The area-based amplification factor  $A_{\text{Cx}}^a$  can be used as an estimate for the integrated charge of a current pulse. However, it has a higher uncertainty ( $\sim 10 \%$ ) than the amplitude-based factor  $A_{\text{Cx}}^Q$  ( $\sim 4 \%$ ) due to the measurement limitations of the oscilloscope.

## 1.1. MEASUREMENT SETUP

---

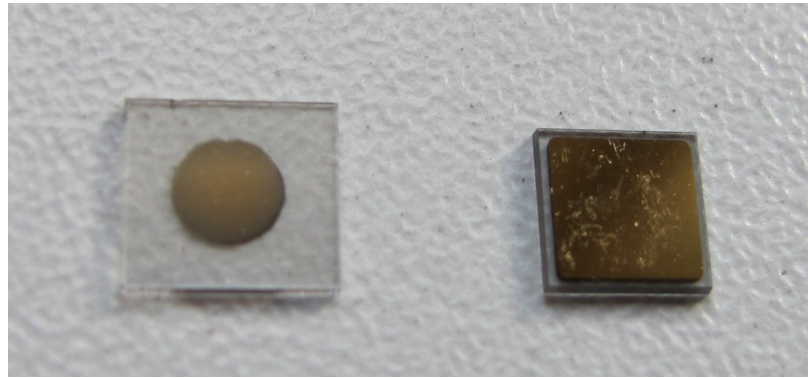


Figure 1.3: Two scCVD diamond samples: A IIa 1scdhq (left) and an E6 S37 (right).

83 **C2 current amplifier** calibration only requires the measurement of the amplitude gain.  
 84 To keep the output signal amplitude within the  $\pm 1$  V linear range of the amplifier, the  
 85 input signal amplitude has to be minimised. The signal from the generator is therefore  
 86 routed through a 36 dB attenuator to decrease its amplitude to  $U_{\text{inAtt}} = (3.95 \pm 0.05)$  mV.  
 87 Two amplifiers with different gains have been measured, because both are used for the  
 88 measurements. The output of the first amplifier amounts to  $U_{\text{C2-1}} = (860 \pm 5)$  mV. This  
 89 yields the amplification gain

$$A_{\text{C2-1}} = \frac{U_{\text{inAtt}}}{U_{\text{C2-1}}} = (217 \pm 3). \quad (1.4)$$

90 The second amplifier has the output equal to  $U_{\text{C2-2}} = (632 \pm 5)$  mV with the resulting gain  
 91 of  $A_{\text{C2-2}} = (152 \pm 3)$ .

### 92 1.1.2 Diamond samples

93 Detector-grade diamonds are very difficult to produce. The major challenge is to ensure  
 94 a high enough purity of the lattice. The sensor samples used for these studies have been  
 95 acquired from Element Six (E6) [?]. They all have the same standard dimensions. sCVD  
 96 diamonds with dimensions  $4.7 \times 4.7$  mm<sup>2</sup> are already sufficiently large for most of the beam  
 97 monitoring applications and still affordable. One sample with dimensions of  $5.6 \times 5.3$  mm<sup>2</sup>  
 98 produced by IIa Singapore [?] has also been characterised at CERN [?]. The target thickness  
 99 for all samples is 500  $\mu\text{m}$ . Diamonds this thick yield a high enough signal-to-noise ratio  
 100 for MIPs to be measured by the available electronics. Table 1.1 shows all the samples used  
 101 for this study. Two of them are measured before and after irradiation and then compared.  
 102 Irradiation doses for damaging the material need to be high – above  $10^{12}$  particles per cm<sup>2</sup>  
 103 to be able to observe a significant change in behaviour of a diamond sensor.

Name	Type	Producer	Dimensions [mm <sup>2</sup> ]	Thickness [ $\mu\text{m}$ ]	Electrode	Irradiated
S37	sCVD	E6	$4.7 \times 4.7$	548	Cr/Au	no
S50	sCVD	E6	$4.7 \times 4.7$	537	Cr/Au	no
S52	sCVD	DDL	$4.7 \times 4.7$	515	DLC/Pt/Au	$3.63 \times 10^{14} \frac{\pi}{\text{cm}^2}$
S79	sCVD	E6	$4.7 \times 4.7$	529	Cr/Au	$1 \times 10^{14} \frac{\pi}{\text{cm}^2}$
ELSC	sCVD	E6	$4.7 \times 4.7$	491	Cr/Au	no
1scdhq	sCVD	IIa	$5.6 \times 5.3$	460	Cr/Au	no

105

Table 1.1: Diamond sensor samples used.

106       The diamond samples have quoted impurity densities of  $\leq 2 \times 10^{14} \text{ cm}^{-3}$  and nitrogen  
107 incorporation of  $\leq 10^{-9}$ . The electrodes were added by various companies and institutes.  
108 For instance, S52 was metallised by a company DDL (now defunct) while the Physics De-  
109 partment of the University of Firenze, Italy metallised the S79. There are also several  
110 techniques for producing the electrodes. The DDL contacts consist of three layers: DLC  
111 (diamond-like carbon)/Pt/Au with 4/10/200 nm thicknesses, respectively. The metallisa-  
112 tion for S79, on the other hand, is made up of Cr/Au with a total thickness of  $\sim 400$  nm.  
113 The area coverage also differs from sample to sample. Diamonds must not be metallised  
114 until the very edge as the proximity of contacts with a high potential may lead to sparking.  
115 However, the areas not covered by the metallisation are less efficient because the fringe  
116 fields at the edges are not as strong as in between the electrodes. This effectively reduces  
117 the sensitive area of the sensors. In the diamonds used here the effective area is anywhere  
118 from  $9 \text{ mm}^2$  to  $18 \text{ mm}^2$ . The leakage current is below 1 nA, but increases for the irradiated  
119 samples. The capacitance is of the order of  $(2.0 \pm 0.3)$  pF.

120     **1.1.3 Readout devices**

121       Electrical signals in diamond detectors are in the GHz frequency range. To preserve the  
122 information in the signals, the readout device with a high bandwidth limit must be used. For  
123 instance, a 250 MHz limit is enough for the spectroscopic measurements with the Cx charge  
124 amplifier, but might be insufficient for the current measurements with the C2 amplifier.

125       Two devices are used take data shown in this chapter. The first choice is a 2 GHz LeCroy  
126 WaveRunner 204MXi-A. This specific model has a sufficiently high bandwidth limit for the  
127 fast current preamplifier signals. It offers a reliable solution for analogue signal readout of  
128 limited amounts of data. However, its slow acquisition speed is a bottleneck in a test beam  
129 experiment. Its initial 100 Hz readout rate decreases to a mere 20 Hz within 20 minutes,  
130 because every single trigger is saved as a separate file and the Windows operating system  
131 is not capable of handling 10000+ files in a single directory easily. This is why it has been  
132 exchanged with a DRS4 [?], an analogue readout device developed by PSI, Switzerland.  
133 This compact device is capable of recording up to four waveforms at a time at a steady  
134 rate of up to 500 Hz. Its 700 MHz bandwidth limitation is sufficient for the signal from the  
135 charge amplifier.

136     **1.1.4 Setup for the  $\beta$  detection efficiency study**

137       The efficiency study of the diamond sensors has been carried out at CERN in the North  
138 Hall test beam facility. There a straight high-energy particle beam of 120 GeV  $\pi$  is provided  
139 to the users to calibrate their detectors. The beam has a transverse spread of  $\sigma = 10$  mm in  
140 both axes. The particle rate is of the order of  $10^4 \pi \text{ cm}^{-2} \text{ s}^{-1}$ . A diamond sensor embedded  
141 in a printed circuit board (PCB) carrier has been placed in the beam spot perpendicular  
142 to the beam and connected via an SMA connector directly to a charge amplifier. The

## 1.1. MEASUREMENT SETUP

---

amplified signal is read out using a LeCroy oscilloscope and a DRS4 analogue readout system. A computer is used as a controller and data storage for the readout device. A beam telescope is used as a reference detector. It is a device that helps to cross-check the measurements of the devices under test (DUTs) and to carry out spatially resolved studies on the DUTs. It consists of several pixellated sensor planes placed in series, which can track a particle's trajectory with a precision of a few  $\mu\text{m}$ . The sensor planes are positioned in front of the DUT and behind it. Then the beam telescope acts as a trigger system – it triggers the readout of both the telescope data and DUT data when both the planes in front and behind the DUT record a hit by an incident particle. A particle detected by all the planes within the DUT window and the DUT itself counts towards its efficiency whereas a hit missed by the DUT means that the DUT is not 100 % efficient. To discard the hits that miss the DUT completely, a region of interest (ROI) can be chosen in the beam telescope planes. The equation for calculating the sensor efficiency is therefore

$$\epsilon = \frac{N_{\text{DUT}} \wedge N_{\text{telescope}}}{N_{\text{telescope}}} \quad (1.5)$$

for an ROI smaller than the sensitive region of the diamond.

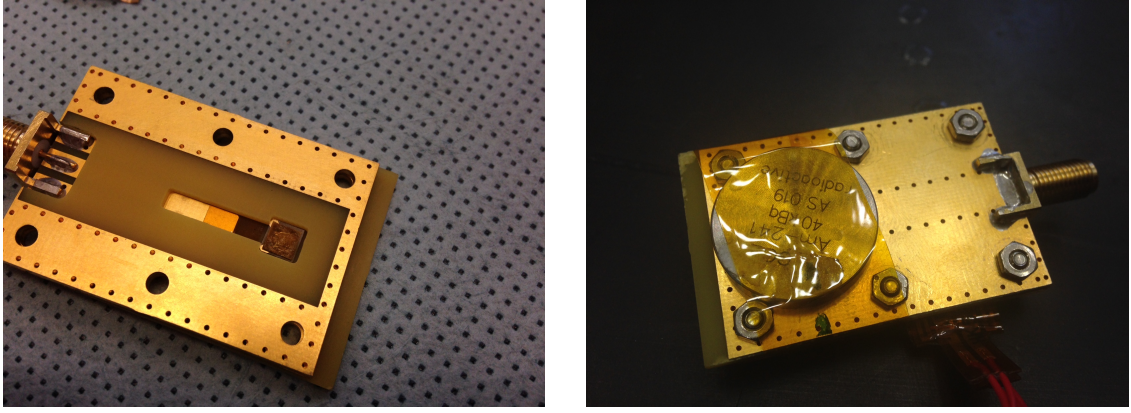
### 1.1.5 Room temperature $\alpha$ -TCT setup

This TCT study is a follow-up of an extensive diamond TCT study at cryogenic temperatures [?]. The room-temperature TCT measurements have been carried out in the laboratory. The setup consists of a diamond sensor embedded in a PCB carrier, a current amplifier and an oscilloscope. To measure  $\alpha$  particles, their energy loss during their trajectory has to be minimised. Therefore the diamond is placed inside a vacuum chamber. The chamber is a steel tube with a diameter of 5 cm. On one side it is connected to a vacuum pump via a steel hose. A feedthrough with an SMA connector is placed on the other side. A CIVIDEC C2 current amplifier is connected directly onto the feedthrough. The amplified output is connected to the oscilloscope via an SMA cable. An  $^{241}\text{Am}$  source with a diameter of 2 cm and a height of 0.5 cm is fixed onto the sensor carrier (figure 1.4a, figure 1.4b). Then the carrier is inserted in the chamber and fixed in place using an air-tight clamp. The pump can then be switched on. It is capable of providing the inside pressure as low as  $10^{-4}$  mbar after approximately one hour of operation.

### 1.1.6 Cryogenic $\alpha$ -TCT setup

The experiment at cryogenic temperatures has been carried out at the Central Cryogenic Laboratory at CERN. The room-temperature TCT setup has to be modified to allow for measurements at temperatures as low as 2 K. It consists of three parts:

1. a cryostat – a thermally insulated cylinder containing liquid helium,
2. an inlet – an air-tight mechanical tube with valves and feedthroughs at the top that is lowered in the liquid helium and



(a) PCB carrier with an embedded diamond sample. (b) Radioactive source over the carrier.

Figure 1.4: Positioning of the  $\alpha$ -source on top of the sensor carrier.

178     3. the diamond sample embedded in a PCB carrier with a fitted temperature sensor, a  
179       heater and cables leading to the feedthroughs.

180     The setup is described in detail in [?].

181     When the diamond sample is placed in the PCB carrier and the  $^{241}\text{Am}$  source is in  
182       place, the inlet is sealed and lowered in the empty cryostat. Then the inside volume of the  
183       inlet is evacuated down to  $10^{-5}$  mbar while the liquid helium is flowing into the cryostat.  
184     To improve the thermal contact between the diamond and the coolant, a small amount of  
185       helium gas is added inside the evacuated inlet, setting the vacuum to around  $10^{-3}$  mbar.  
186     This value changes with time, because the gas condenses on the walls of the inlet, reducing  
187       the number of floating particles. For this reason the helium gas has to be added on an  
188       irregular basis. Every addition causes a significant undershoot of the sample temperature,  
189       which has to be corrected for using a heater placed on the back of the PCB carrier. Also,  
190       the added gas deteriorates the vacuum inside the inlet. Furthermore, at approximately 60 K  
191       the helium gas has to be evacuated from the inlet to avoid a potential explosion due to the  
192       expansion of the gas with temperature.

193     When the sample is cooled to 4.2 K, the minimum temperature achievable by means  
194       of liquid helium without over-pressurising it, the measurements can begin. A temperature  
195       sensor placed on the back of the PCB carrier is used to measure the temperature of the  
196       sample. After every temperature data point, the current through the heater placed in  
197       the PCB next to the diamond sample is increased, increasing the sample. The initial  
198       temperature time constant of the order of tenths of seconds at low temperatures increases  
199       with temperature. Even more so when helium is evacuated from the inlet at 60 K, removing  
200       the thermal bridge between the wall of the inlet and the diamond sample. At the room  
201       temperature (RT), the time constant is already of the order of minutes.

<sup>202</sup> **1.2 Charged particle pulses and spectra**

<sup>203</sup> In previous chapter the ionisation profiles for different types of radiation were discussed.  
<sup>204</sup>  $\beta$  radiation induces a triangular electric pulse whereas  $\alpha$  radiation induces a rectangular  
<sup>205</sup> one. However, their amplitude, width and rise/fall time depend heavily on the type of  
<sup>206</sup> interaction with the diamond, the purity of the diamond and the bandwidth of the amplifier  
<sup>207</sup> and the oscilloscope. This section shows the signal pulses of  $\alpha$ ,  $\beta$  and  $\gamma$  radiation with their  
<sup>208</sup> respective energy distributions for the case of a diamond detector.

<sup>209</sup> Figure 1.5 shows a set of pulses and an averaged waveform for 5.5 MeV  $\alpha$ , 2.3 MeV  
<sup>210</sup>  $\beta$  and 1.3 MeV  $\gamma$  radiation using an  $^{241}\text{Am}$ , a  $^{90}\text{Sr}$  and a  $^{60}\text{Co}$  source, respectively. The  
<sup>211</sup> particles are measured with the non-irradiated sCVD diamond S37.  $\alpha$  particles always  
<sup>212</sup> produce the same signal pulse, but with a high noise RMS. The averaging suppresses the  
<sup>213</sup> noise while retaining most the information. It does, however, smear the rising and falling  
<sup>214</sup> edge, increasing the rising and falling time. The  $t_r$  is now of the order of 0.5 ns. Both  $\beta$   
<sup>215</sup> and  $\gamma$  pulses look similar - triangular and with a wide range of amplitudes. Here the pulse  
<sup>216</sup> count is low, so the pulses with a high amplitude are not recorded. A trigger would need  
<sup>217</sup> to be set very high to “catch” them with the oscilloscope.

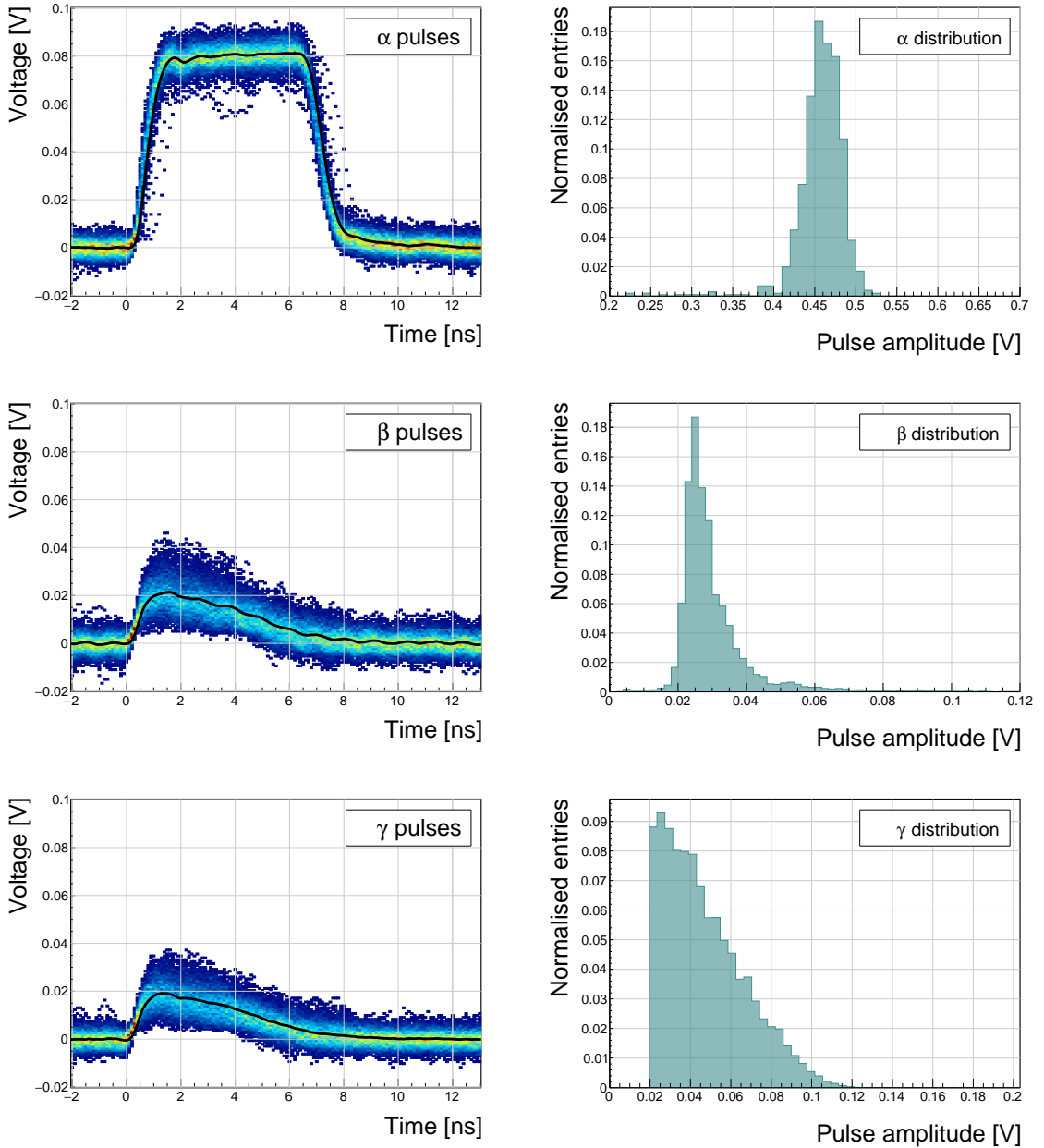


Figure 1.5: Superimposed and averaged pulses (left figures, current amplifier) and distributions of deposited energy (right figures, charge amplifier) for three types of radiation. Note the scale on the X axis of the distributions.

<sup>218</sup> **1.3 Radiation limitations**

<sup>219</sup> This section quantifies the decrease in charge collection efficiency as well as the effects on  
<sup>220</sup> long-term measurement stability in irradiated sCVD diamonds.

<sup>221</sup> **1.3.1 Irradiation study**

<sup>222</sup> This subsection contains a study of the effects of 300 MeV pion ( $\pi$ ) irradiation on the charge  
<sup>223</sup> collection efficiency of sCVD diamond detectors. To carry out this study, two diamond  
<sup>224</sup> samples were irradiated to doses of  $1 \times 10^{14} \pi \text{ cm}^{-2}$  (S79) and to  $3.63 \times 10^{14} \pi \text{ cm}^{-2}$  (S52).  
<sup>225</sup> A test beam campaign was carried out to observe the charge collection efficiency at different  
<sup>226</sup> bias voltage settings. The efficiency values acquired are used to determine the effective drop  
<sup>227</sup> in efficiency as a function of the received radiation dose. This is to test if the collected charge  
<sup>228</sup>  $Q$  is inversely proportional to the received dose  $\Phi$ . A procedure defined by a collaboration  
<sup>229</sup> researching diamond behaviour RD42 has been applied to the measured values to extract  
<sup>230</sup> the damage factor described in ??.

<sup>231</sup> The following subsection contains measurements and results of a long-term stability  
<sup>232</sup> study using  $\alpha$  and  $\beta$  particles. In particular, the charge collection efficiency with  $\beta$  and  $\alpha$   
<sup>233</sup> radiation as a function of time is measured. To investigate this effect on the scale of charge  
<sup>234</sup> carriers, the change of TCT (transient current technique) pulses with time is observed.  
<sup>235</sup> Finally, a procedure that improves the pulse shape and with it the charge collection is  
<sup>236</sup> proposed.

<sup>237</sup> **Irradiation with a 300 MeV  $\pi$  beam**

<sup>238</sup> The samples were irradiated at the Paul Scherrer Institute (PSI) [?] by means of a beam  
<sup>239</sup> of pions with an energy of 300 MeV (kinetic energy 191.31 MeV) and with a flux of up  
<sup>240</sup> to  $1.5 \times 10^{14} \pi \text{ cm}^{-2}$  per day. The system has a 10 % uncertainty on the beam energy.  
<sup>241</sup> Looking at the pion damage curve in figure ??,  $\pi_{300 \text{ MeV}}$  point (191 MeV kinetic energy)  
<sup>242</sup> sits on a steep section of the DPA curve. This means that a deviation in beam energy can  
<sup>243</sup> have a significant effect on the damage in the sensor. In addition, their quoted uncertainty  
<sup>244</sup> on the measurement of the delivered dose is  $\pm 20 \%$ .

<sup>245</sup> Two diamond samples, S52 and S79, were put in the  $\pi_{300 \text{ MeV}}$  beam in the 2014 PSI  
<sup>246</sup> irradiation campaign; S52 to  $(1 \pm 0.21) \times 10^{14} \pi \text{ cm}^{-2}$  and S79 to  $(3.63 \pm 0.77) \times 10^{14} \pi \text{ cm}^{-2}$ .  
<sup>247</sup> During the process, the gold electrodes got slightly activated, but the activation decayed in  
<sup>248</sup> two weeks.

<sup>249</sup> **300 MeV  $\pi$  radiation damage factor**

<sup>250</sup> Three diamonds – non-irradiated S37 and irradiated S52 and S79 – were tested in a  $\pi_{120 \text{ GeV}}$   
<sup>251</sup> test beam in the SPS North Experimental Area at CERN [?] before and after irradiation.  
<sup>252</sup> The goal was to estimate the charge collection efficiency and charge collection distance as a  
<sup>253</sup> function of irradiation dose. The samples were primed (pumped) prior to data taking using

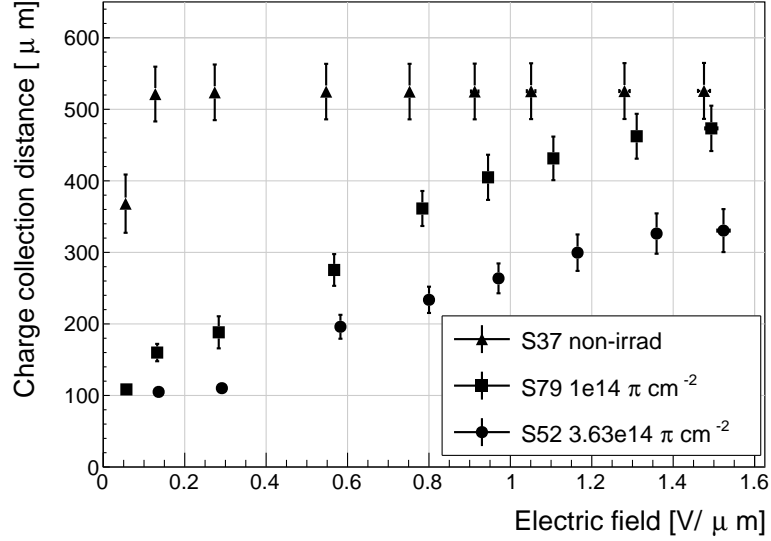


Figure 1.6: The figure shows the CCD for S37, S79 and S52 at a range of bias voltage settings.

a  $^{90}\text{Sr}$  radioactive source. The data were then taken at a range of bias voltages ranging from 30 V to 900 V, yielding between  $0.06 \text{ V}/\mu\text{m}$  and  $1.8 \text{ V}/\mu\text{m}$  electrical field in the bulk. Every data point contained approximately  $5 \times 10^4$  measured particles. The charge deposited by the particles was measured using a CIVIDEC Cx charge preamplifier.

As expected, the integrated amplitude spectrum is a Landau distribution. Its most probable value (MPV) is used to calculate the most probable collected charge  $Q_i$ :

$$Q_i [\text{e}^-] = \frac{1}{1.6 \times 10^{-19}} Q_i [\text{C}] = 6241 \cdot Q_i [\text{fC}] = 6241 \cdot \frac{\text{MPV} [\text{mV}]}{A [\frac{\text{mV}}{\text{fC}}]}, \quad (1.6)$$

where  $A = 9.3 \text{ mV/fC}$  is the preamplifier gain factor and  $1 \text{ e}^- = 1.6 \times 10^{-19} \text{ C}$ .

The CCD for the three measured samples at a bias voltages ranging from  $0.2\text{--}1.6 \text{ V } \mu\text{m}^{-1}$  calculated using equation ?? is shown in figure 1.6. S37 exhibits a full collection distance already at  $0.4 \text{ V } \mu\text{m}^{-1}$  whereas the irradiated samples have a more gentle increase of CCD with increasing bias voltage. It is evident that at  $1 \text{ V } \mu\text{m}^{-1}$  the maximum CCD has not been reached in the case of S79 and S52. Nevertheless, to compare the measured data point with those provided by RD42, the CCD at  $1 \text{ V } \mu\text{m}^{-1}$  has to be taken.

The data points with the maximum CCD obtained in the test beam measurements are plotted against received radiation dose in figure 1.7. Equation ?? is fitted to the data points and a damage factor  $k_\lambda = (4.4 \pm 1.2) \times 10^{-18} \mu\text{m}^{-1} \text{ cm}^{-2}$  is obtained. The value is for a factor of two higher than the damage factor obtained by RD42. This could be due to an insufficient priming time ahead of the measurement. In addition, the diamond samples have not been polished and re-metallised after irradiation, as is the case for the RD42. Also, with only two samples measured, the statistical uncertainty is high. Nevertheless, it can be

### 1.3. RADIATION LIMITATIONS

---

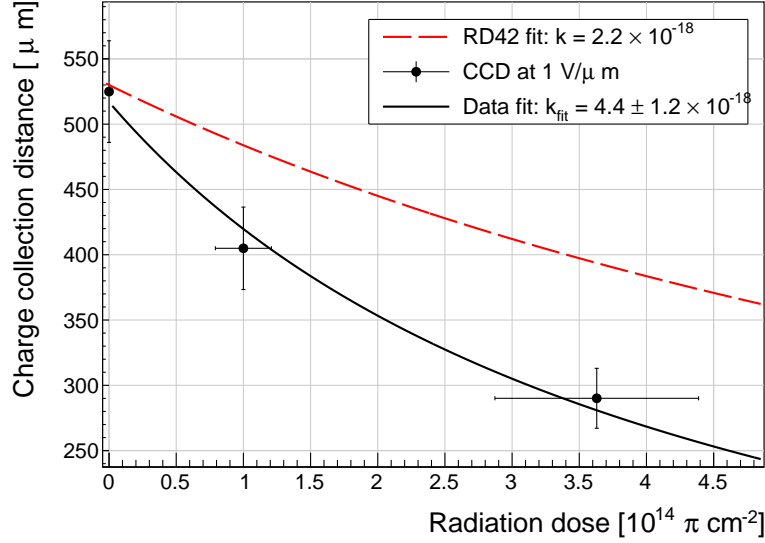


Figure 1.7: The charge collection distance at 1 V/ $\mu\text{m}$  bias voltage for the three diamond samples is plotted as a function of the received radiation dose. It is compared to the RD42 data for pion irradiation. The data points are about 15–25 % lower than expected from the RD42 data [?].

<sup>274</sup> concluded that the 300 MeV pions damage the diamond bulk significantly more than the  
<sup>275</sup> 24 GeV protons.

<sup>276</sup> **1.3.2 Long-term measurement stability**

<sup>277</sup> An important requirement for particle detectors is a stable performance over long periods  
<sup>278</sup> of time. For instance, the charge collection for a defined radiation type and quantity must  
<sup>279</sup> not change over time or has to change in a predicted way. The stability of diamond detec-  
<sup>280</sup> tors depends on many factors, e.g. material purity, polishing process, electrode material,  
<sup>281</sup> irradiation damage etc. The aim is to study the behaviour of diamond under controlled con-  
<sup>282</sup> ditions, with the goal to understand its limitations. One of these limitations is the received  
<sup>283</sup> radiation dose as it can affect the long-term stability of the sensor during operation.

<sup>284</sup> The three diamond samples (S37, S79 and S52) have been exposed to two different types  
<sup>285</sup> of ionising radiation for a longer period to see if their behaviour changes over time. Two  
<sup>286</sup> parameters have been observed in particular:

- <sup>287</sup>
1. Charge collection of  $\beta$  particles and
  - <sup>288</sup> 2. Charge collection and ionisation profile of  $\alpha$  particles.

<sup>289</sup>  **$\beta$  long-term stability**

<sup>290</sup> The diamond samples have undergone a long-term stability test at room temperature using  
<sup>291</sup>  $\beta$  radiation. This has been done using a  ${}^{90}\text{Sr}$  source emitting  $\sim$ 2.28 MeV electrons at a

rate of approximately  $10^4 \text{ e}^- \text{ cm}^{-2}$ . To simulate the initial conditions in HEP experiments, the sensors must not be primed before starting the measurements. The measurement setup consists of a diamond sample (S37, S52 or S79) with the CIVIDEC Cx spectroscopic amplifier, a silicon diode with a CIVIDEC C6 amplifier for triggering and a  $^{90}\text{Sr}$  source on top. A particle emitted by the source traverses the sensor bulk and hits the silicon diode, triggering the analogue signal readout. The source is left on the top for the course of the experiment. The measurements, however, are taken at discrete times. For every data point, approximately  $10^4$  triggers have to be recorded. The offline analysis of the recorded signal pulse amplitudes yields a Landau distribution for every data point. The current charge collection relative to the initial charge collection for every sample is plotted as a function of the received  $\beta$  dose in figure 1.8. It shows that, for the irradiated samples, the charge collection efficiency improves when the diamond sensor is primed with a  $\beta$  source. The effect is negligible for the non-irradiated high-quality S37. Both relative increases are significant – 22 % for S79 and 55 % for S52. At a received dose of approximately  $4 \times 10^6$  particles the charge collection is stabilised. At that point S79 achieves close to a full efficiency (in absolute values – not shown) whereas S52 reaches approximately 50 %.

The  $\sim 2.28 \text{ MeV}$  electrons emitted by this source are not MIPs; their charge deposition is higher than that of an electron MIP, according to the Bethe-Bloch distribution [?]. Nevertheless, for the purpose of these measurements this energy is adequate since only the relative change in charge collection is of interest.

To sum up, diamond provides a stable measurement of the  $\beta$  radiation detection after reaching a stable state. Even if damaged by radiation, it reaches a stable charge collection at a received dose of  $\sim 4 \times 10^6$  MIPs. Its efficiency decreases with a high irradiation dose. However, the decrease can be accounted for if the damage factor and the rate and energy of the particles are known.  $\gamma$  radiation has a similar impact on the diamond as the  $\beta$ . The incident photons, if they interact with the diamond, prime the bulk, increasing the charge collection efficiency. The difference, however, is that the interaction probability (cross-section) is lower for gammas [?, ?].

### $\alpha$ long-term stability

This part discusses the stability of irradiated diamond sensors during  $\alpha$  measurements. An  $^{241}\text{Am}$  source has been used, emitting  $\alpha$  particles with a mean energy of 5.5 MeV.

To test the stability of the diamond during  $\alpha$  measurements, the samples have been biased at  $+500 \text{ V}$  and exposed to up to 8000  $\alpha$  hits while measuring their charge collection efficiency using the CIVIDEC Cx spectroscopic amplifier. The charge collected at every measurement point  $Q(\Phi)$  is compared to collected charge of the first measurement  $Q(0)$ . The resulting ratio  $\frac{Q(\Phi)}{Q(0)}$  for all samples is shown in figure 1.9. Each measurement point is an average of 30 consecutive  $\alpha$  hits. The observations are the following:

- $Q(\Phi)$  for the non-irradiated S37 is stable as compared to  $Q(0)$  over the course of the measurement.
- The initial efficiency of the irradiated S52 and S79 starts decreasing already at a low

### 1.3. RADIATION LIMITATIONS

---

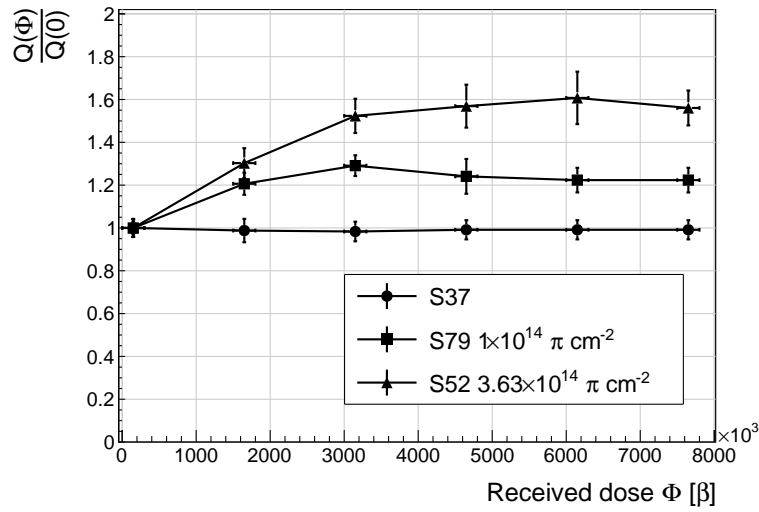


Figure 1.8: Relative increase of charge collection over time due to priming with the  $^{90}\text{Sr}$  radioactive source. The charge collection for the non-irradiated S37 stays constant. The bias voltage for this measurement is 1 V/ $\mu\text{m}$ .

332         $\alpha$  count.

- 333        - The charge collection efficiency of the unprimed irradiated samples drops much faster  
334        than after priming.
- 335        - The particle count rate decreases with decreased efficiency, which is clearly seen in the  
336        unprimed S52 data where the data points at a low efficiency are much further apart.

337        The absolute values are not shown here because only the relative drop is of interest in the  
338        scope of the long-term stability tests.

339         $\alpha$  affect the irradiated diamond differently than when subjected to  $\beta$  radiation. This  
340        can be due to several contributions:

341        **Quantity of deposited energy.** The deposited energy on its path produces 24 times  
342        more e-h pairs than that of a MIP, according to equations ?? and ???. Such a difference  
343        may affect the charge collection efficiency due to saturation.

344        **A point-like charge carrier creation.** The energy of an  $\alpha$  particle is deposited in a  
345        small volume – 14  $\mu\text{m}$  in depth and  $\sim 20$  nm radially [?]. A dense distribution of charge  
346        carriers might affect their behaviour at the start of the drift.

347        **Single-polarity charge carriers.** Carriers of only one polarity drift through the sensor  
348        while those of the opposite polarity almost instantly reach the adjacent electrode. Therefore  
349        the charges only one polarity get trapped along the drift path, contributing to a single-  
350        polarity space-charge build-up.

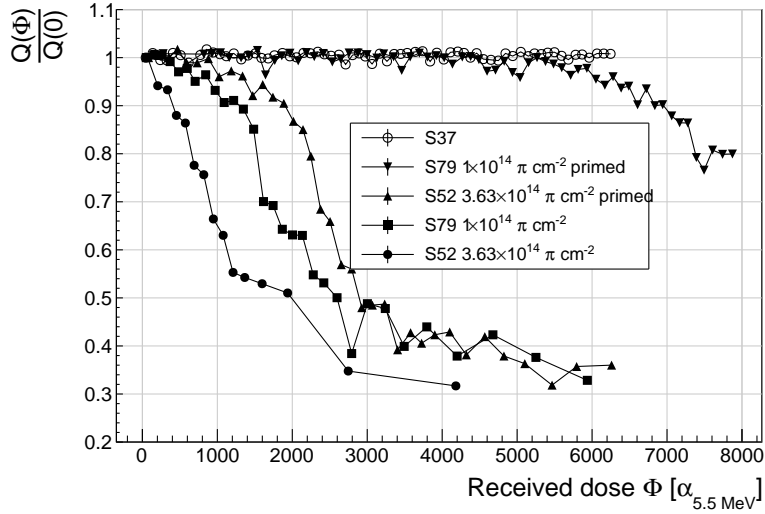


Figure 1.9: A relative drop in charge collection efficiency as a function of the received  $\alpha$  dose for non-irradiated and irradiated diamond samples.

351 To investigate this sudden drop in efficiency, the current pulse shapes using a CIVIDEC  
 352 C2 current amplifier have to be observed, as shown in figure 1.10. The shape of the pulse  
 353 holds more information about the charge carrier properties in the sensor than solely the  
 354 value of the integrated charge. This time only the primed S79 sample has been tested.  
 355 Both the hole and the electron collection are observed to determine whether they behave  
 356 differently or not.

357 The first observation of the raw acquired data in figures 1.10 is that the initially stable  
 358 pulses start deteriorating; several different shapes start appearing gradually, some still very  
 359 similar to those from the beginning while the others with almost zero amplitude.

360 A more dedicated analysis of the first observation has been carried out as follows: at  
 361 the beginning of the test when the diamond is still operating stably, 60 pulses are recorded.  
 362 An average pulse is calculated. This is a reference pulse for the subsequent measurement  
 363 points. Then an RMS of the individual pulses  $\sigma_n$  with respect to the reference pulse is  
 364 calculated and the resulting RMS values are summed together into  $\sigma_{\text{ref}}$ :

$$\sigma_{\text{ref}} = \sum_{n=1}^{60} \sigma_n. \quad (1.7)$$

365 All the subsequent data points also consist of a set of 60 pulses. At every data point the  
 366 summation of the RMS values of the individual pulses with respect to the initial averaged  
 367 pulse  $\sigma$  is calculated according to equation 1.7. The ratio between the initial  $\sigma_{\text{ref}}$  and  
 368 discrete values  $\sigma$  gives a measure of the change of the pulse shape with respect to the  
 369 reference pulse at the start of the measurement. Therefore the initial value is 1 and it  
 370 decreases if the RMS values of subsequent data points are higher. Figure 1.11 shows the  
 371 ratio  $\frac{\sigma_{\text{ref}}}{\sigma(\alpha \text{ dose})}$ . From the data obtained it can be concluded that the initial pulse shape

### 1.3. RADIATION LIMITATIONS

---

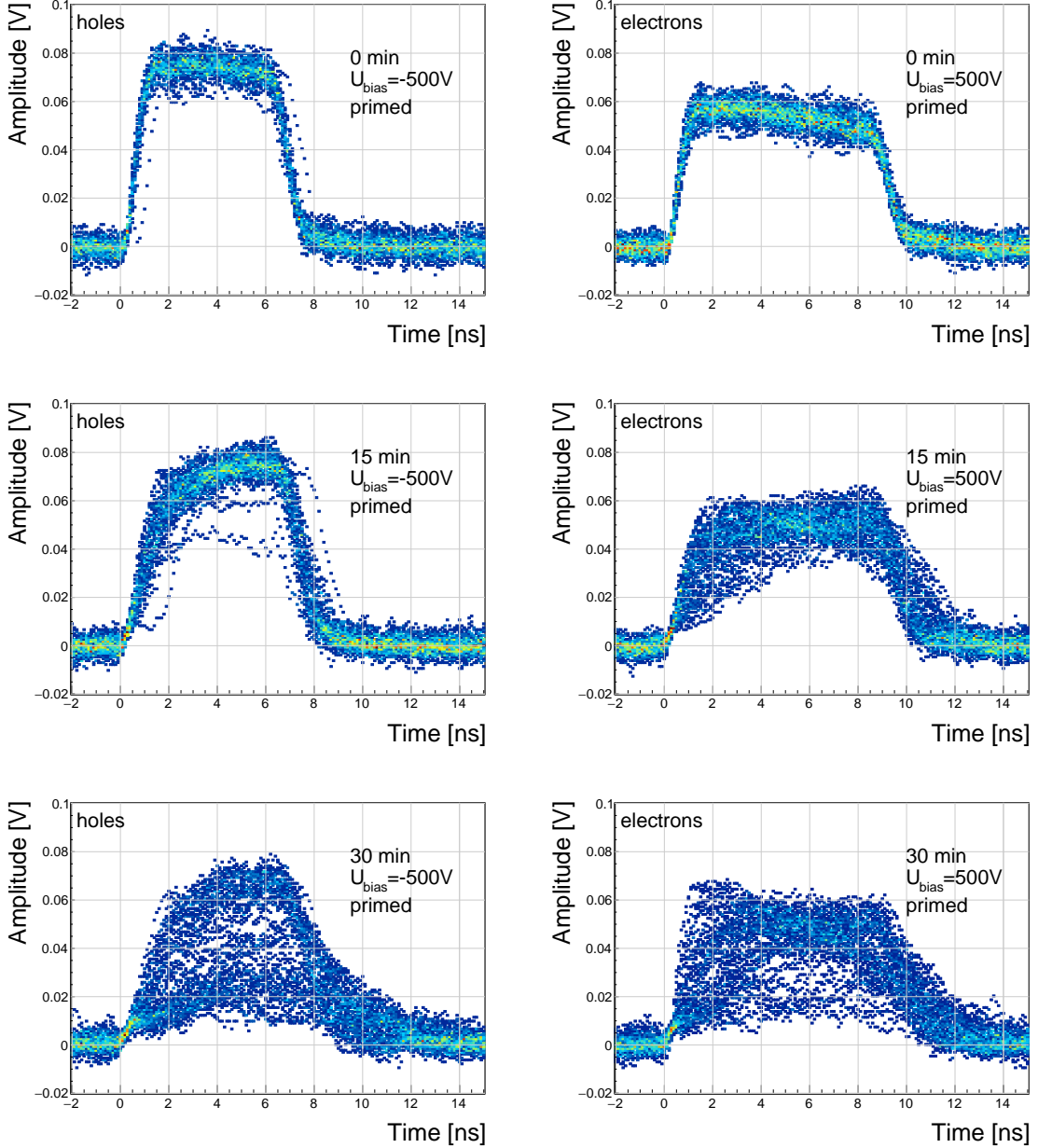


Figure 1.10: The signal of the irradiated and primed S79 deteriorates with time for both polarities. Every plot contains 60 superimposed pulses.

372 quickly starts deteriorating. In fact, the deterioration of the shape follows an approximate  
 373 exponential decay function, which can be fitted to the data. The resulting decay constants  
 374 for electrons and holes are  $\tau_e = (4400 \pm 150) \alpha^{-1}$  and  $\tau_h = (3300 \pm 140) \alpha^{-1}$ . The electrons  
 375 retain the initial shape for longer. The deteriorated shapes also seem to be for a factor of  
 376 2 better than those of the holes.

377 **Discussion** One hypothesis is that this behaviour is caused by space-charge build-up.

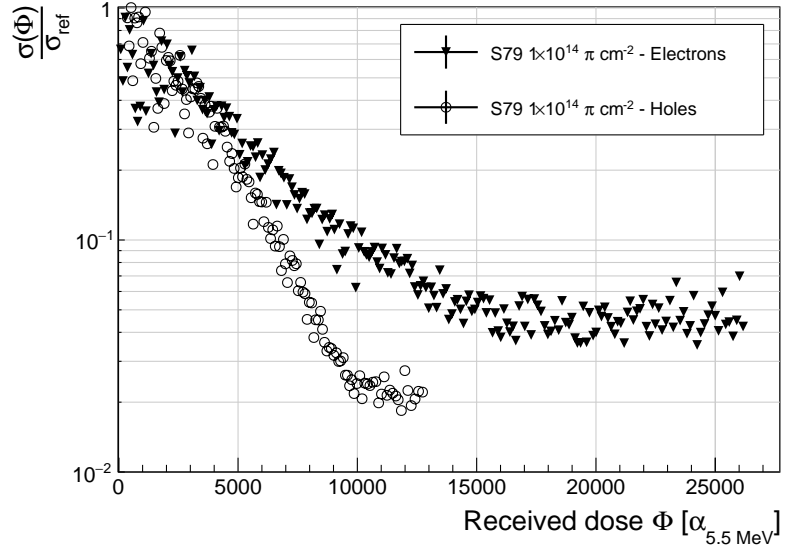


Figure 1.11: Deterioration of the pulse shapes with time.

378 Charge carriers get stopped in the charge traps in the bulk for a long time, building up  
 379 regions of space-charge. The built up space-charge affects the electric field. The field in  
 380 turn affects the drifting charge carriers, slowing them down or speeding them up, depending  
 381 on the field gradient. Since the movement of the carriers is inducing the electric current,  
 382 the field gradient can be observed in the current signal.

383 The fact that the signal shapes vary significantly might be due to a very non-uniform electric  
 384 field, which is created by the three competing processes discussed above. The charge carriers  
 385 are created in a small volume whereby some immediately get trapped, some recombine to  
 386 form excitons ?? and others start drifting. The remaining charge carriers drift towards their  
 387 respective electrodes. Both are trapped on their way, causing the space-charge build-up of  
 388 one polarity on the first 14  $\mu\text{m}$  and of the other polarity all along the sensor thickness. A  
 389 resulting electric field is very non-uniform, which explains the unstable current pulses.

390 **Restoring the pulse shapes** Finally, an effort has been made to find a way for the pulse  
 391 shapes to return to their initial state. Five methods are listed:

- 392 1. No source, with bias voltage,
- 393 2. No source, without bias voltage,
- 394 3. Priming with  $\gamma$  at a rate of  $400 \text{ s}^{-1}\text{cm}^{-1}$  without bias voltage,
- 395 4. Priming with  $\beta$  at a rate of  $1000 \text{ s}^{-1}\text{cm}^{-1}$  with bias voltage and
- 396 5. Priming with  $\beta$  at a rate of  $1000 \text{ s}^{-1}\text{cm}^{-1}$  without bias voltage.

397 Before starting each method, the diamond sample S79 is first primed using a  $^{90}\text{Sr}$  source for  
 398 approximately one hour. Then the bias voltage is switched on and an  $^{241}\text{Am}$  source is put  
 399 on top. The pulses produced by the incident  $\alpha$  particles have a proper rectangular pulse

### 1.3. RADIATION LIMITATIONS

---

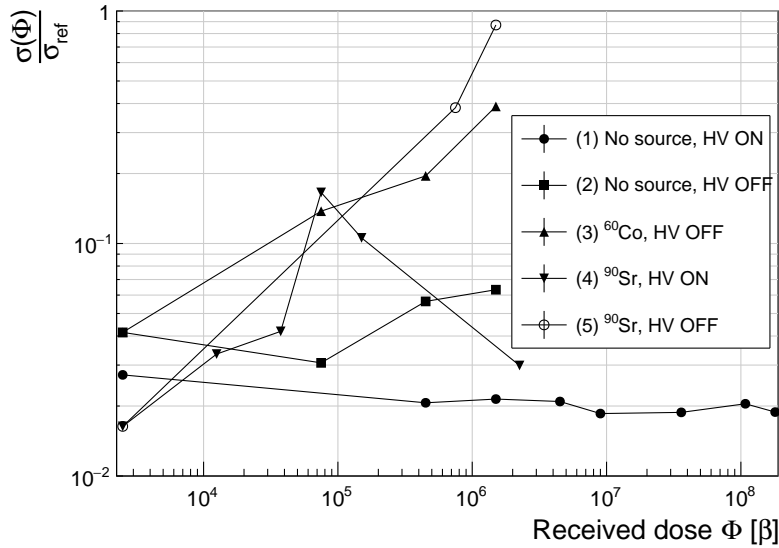


Figure 1.12: Comparison of the five procedures for the “healing” process for an irradiated diamond that had been exposed to  $\alpha$  radiation with a rate of  $10^1 \text{ s}^{-1}$ , with the bias voltage switched on, for at least 30 minutes.

400 at the beginning, but then start changing – first gradually and later increasingly more in  
 401 an erratic way, as described in the text above. After approximately 30 minutes, one of the  
 402 methods is tested. When a “healing” procedure is started, a set of 60 pulses is taken at  
 403 irregular points of time to observe the change in the pulse shape and to assess the quality  
 404 of the “healing” procedure. Then the bias voltage is switched off and the sample is primed  
 405 again to reset its state before starting with the next run.

406 The results depicted in figure 1.12 show that the methods (3) and (5) improve the shape,  
 407 method (2) helps slowly, (1) does not show any change with time and (4) at first improves,  
 408 but then significantly degrades the shape. The effect observed in method (4) has already  
 409 been described in [?]. The “healing” process therefore depends on the rate of radiation, the  
 410 bias voltage and the time of exposure. The ionising radiation creates free charges, which  
 411 quickly recombine close to the place of generation. It is likely that they also release the  
 412 charges trapped during the measurement, reducing the overall effect of the space-charge.  
 413 The traps get filled with both flavours of carriers, thus they are neutralised. The pulse  
 414 shape gradually returns to its initial state.

415

Procedure	Source	Type of radiation	Bias voltage	Effectiveness
1	/	/	ON	no
2	/	/	/	slow
3	$^{60}\text{Co}$	$\gamma$	/	YES
4	$^{90}\text{Sr}$	$\beta$	ON	no
5	$^{90}\text{Sr}$	$\beta$	/	YES

416 Table 1.2: Effectiveness of healing procedures.

<sup>417</sup> **Summary** The shape of the pulses caused by  $\alpha$  radiation changes with time for irradiated  
<sup>418</sup> samples. The shape of the pulses gets distorted and becomes erratic. The charge collection  
<sup>419</sup> decreases and its spread increases. The signal shapes are probably affected by a non-uniform  
<sup>420</sup> electric field, which is caused by the build-up of space charge. The signal degradation  
<sup>421</sup> happens even faster for non-primed diamonds. To “heal” the diamond – to bring the pulse  
<sup>422</sup> shapes back to their initial shape – the sample must be primed using a  $\beta$  or a  $\gamma$  source for  
<sup>423</sup> several minutes without bias voltage. Switching to the inverse polarity for a few seconds  
<sup>424</sup> helps a bit, but in a long run distorts the signal, preventing it from returning to the initial  
<sup>425</sup> shape.

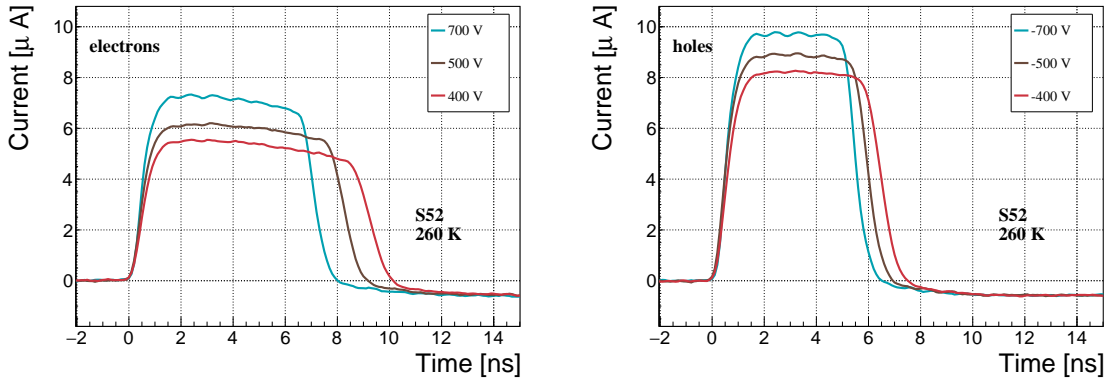


Figure 1.13: Varied bias voltage at a fixed temperature.

## 426 1.4 Temperature limitations

427 A test has been carried out to evaluate the effect of temperature changes on the output  
 428 signal of the diamond sensors. A cryostat filled with liquid helium is used to cool down  
 429 the sensor during the measurement process. The current signal response to  $\alpha$ -particles is  
 430 measured at 18 temperature points between 4 K and 295 K. At every temperature point  
 431 a set of 300 pulses is recorded at various bias voltages. The resulting data show that the  
 432 charge collection is stable from RT down to 150 K where it starts decreasing. It stabilises  
 433 again at about one third of the initial value at 75 K. This behaviour was first measured and  
 434 discussed by H. Jansen [?].

### 435 1.4.1 Temperature-variant $\alpha$ -TCT before irradiation

436 Three sCVD diamond samples have been tested at a range of temperatures using the  $\alpha$ -  
 437 TCT technique. At each temperature point, the bias voltage is set to several positive and  
 438 negative values. A set of 300 pulses is recorded at every data point and averaged offline.  
 439 The resulting averaged pulses of sample S37 at the 260 K temperature point and a bias  
 440 voltage of  $\pm 700$  V,  $\pm 500$  V and  $\pm 400$  V are shown in figure 1.13. The pulses induced by  
 441 holes as charge carriers are shorter than those induced by electrons, which means that holes  
 442 travel faster in diamond. The area of the pulse, however, is the same for both polarities,  
 443 which corresponds to the fact that the same amount of charges is drifting in both cases.

444 Figure 1.14 shows pulses at a bias voltage set to  $\pm 500$  V across the range of tempera-  
 445 tures between 4 K and 295 K. Several conclusions can be drawn by observing their shape.  
 446 First, the pulse shapes change with decreasing temperature. The pulse time gets shorter  
 447 and higher, hinting at the faster carrier drift velocity  $v_{\text{drift}}$ . Second, between 150 K and  
 448 75 K there is a significant change in shape - the time constant of the rising edge increases  
 449 significantly and the pulse area decreases. From 75 K down to 4 K there is no significant  
 450 change. Last, the top of the pulse at the S52 is not flat, which means that a portion of  
 451 the drifting charge is lost along the way. This is due to charge trapping, likely by means of

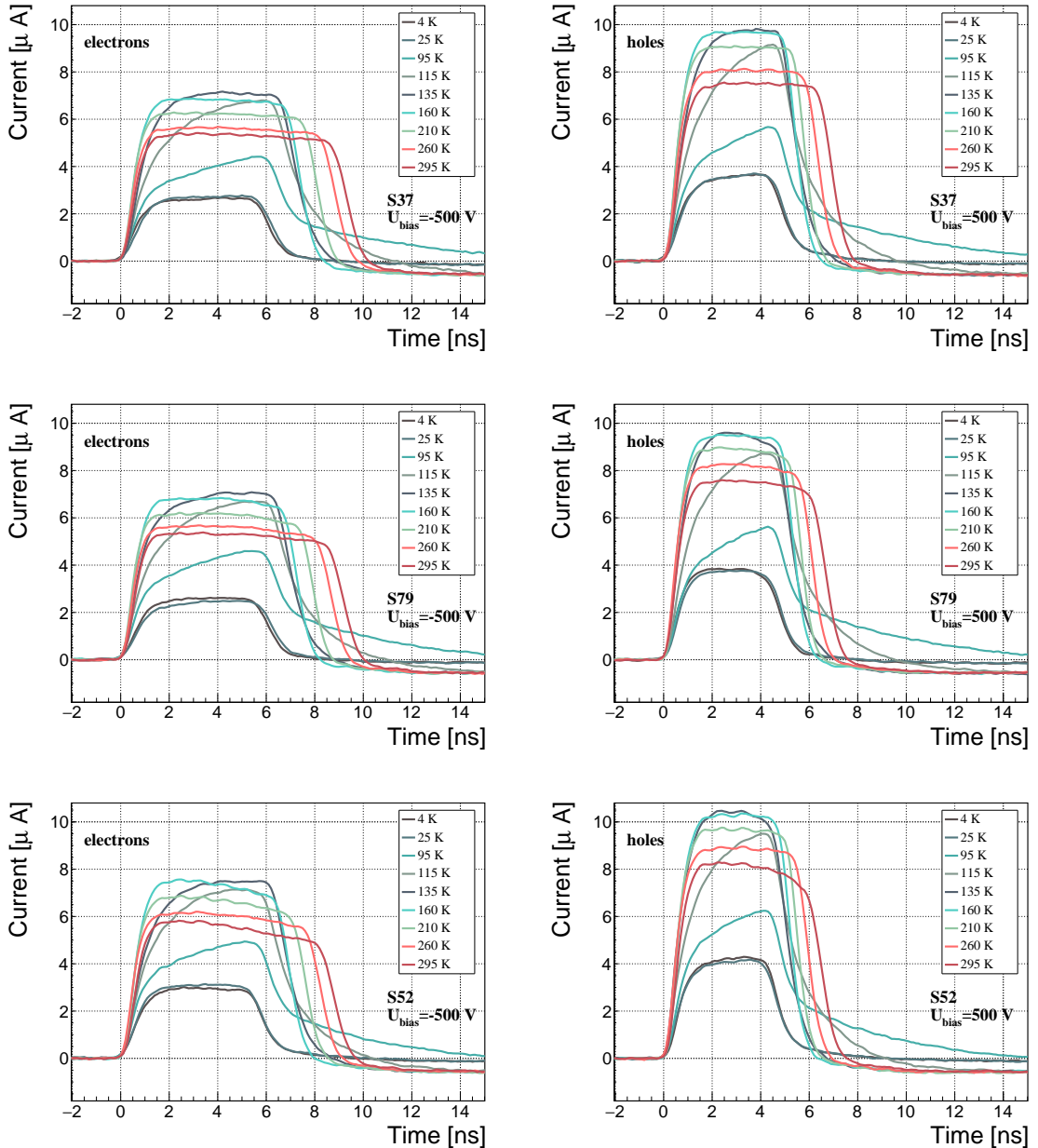


Figure 1.14: Several data points between 4 K and 295 K at a bias voltage of  $\pm 500$  V. The tilted top of the pulse on the bottom left figure is due to built-up space charge.

## 1.4. TEMPERATURE LIMITATIONS

---

452 crystal defects or impurities.

### 453 1.4.2 Temperature-variant $\alpha$ -TCT after irradiation

454 The irradiated S79 and S52 have been re-tested in the cryostat after irradiation. The aim  
455 is to observe how their pulse shapes change with decreasing temperature, in particular the  
456 decaying top of the pulses, as shown in figure 1.15. The decay time gives information on  
457 trapping of charge carriers while travelling through the diamond bulk. A variation of the  
458 decay time constant as a function of temperature might help to reveal the type and depth  
459 of the charge traps. To observe these effects or lack thereof, a number of requirements  
460 have to be met. First, the diamond samples are intentionally not primed prior to the  
461 experiment because priming would improve the pulse shapes and possibly change the decay  
462 time constant of the signal. Second, keeping in mind that the pulse shape of irradiated  
463 diamonds changes with time, the duration of the measurement of an individual data point  
464 has to be short – of the order of 30 seconds. Last, the sequence of the bias voltage settings  
465 is important, the reason for which is explained below.

466 Unfortunately it is not possible to avoid temporal pulse changes. For instance, one  
467 measurement point takes approximately one minute. After the measurement, the bias  
468 voltage polarity is swapped for a few seconds to bring the diamond back into its initial state.  
469 But a few seconds with respect to a minute are not enough, but due to time constraints  
470 this cannot be avoided. Therefore when the bias voltage is set to the next value, there is  
471 still some residual effect of the previous measurement. Similar to the effects of polarisation,  
472 this effect is also decreasing the pulse height. This can be observed in figure 1.15, which  
473 shows the resulting pulses of S52 for bias voltages of  $\pm 200$  V,  $\pm 300$  V,  $\pm 400$  V and  $\pm 500$  V  
474 at 230 K and 260 K. In this case the measurement sequence is: 230K (200 V, 300 V, 400 V,  
475 500 V, -500 V, -400 V, -300 V), 260 K (-200 V, -300 V, -400 V, -500 V, 500 V, 400 V,  
476 300 V). The changes in pulse shapes for holes at 230 K and 260 K cannot be attributed to  
477 the temperature change. Instead, the explanation could lie in diamond “polarisation”. This  
478 means that, when exposed to an electric field with  $\alpha$  measurements ongoing, an internal  
479 electric field of inverse polarity builds up in the diamond, which effectively reduces the  
480 overall electric field. This internal field does not dissipate when the external bias voltage  
481 is switched off. The diamond becomes “polarised”. When switching the polarity of the  
482 external bias voltage, the internal and external electric field point in the same direction at  
483 the beginning, increasing the overall electric field and with it the pulse height. In figure 1.15  
484 this happens when switching from 500 V (figure 1.15a) to -500 V (figure 1.15b) at 230 K.  
485 The built up polarisation contributes to the pulse having a sharp rising edge and a high  
486 amplitude. This effect decays during the next two voltage points. There would be a handful  
487 of ways to avoid this polarisation effect in the data:

- 488 1. After every data point invert the bias voltage and leave it to return to a neutral state  
489 for the same amount of time,
- 490 2. Make a hysteresis of data points, going from minimum negative to maximum positive  
491 bias several times,

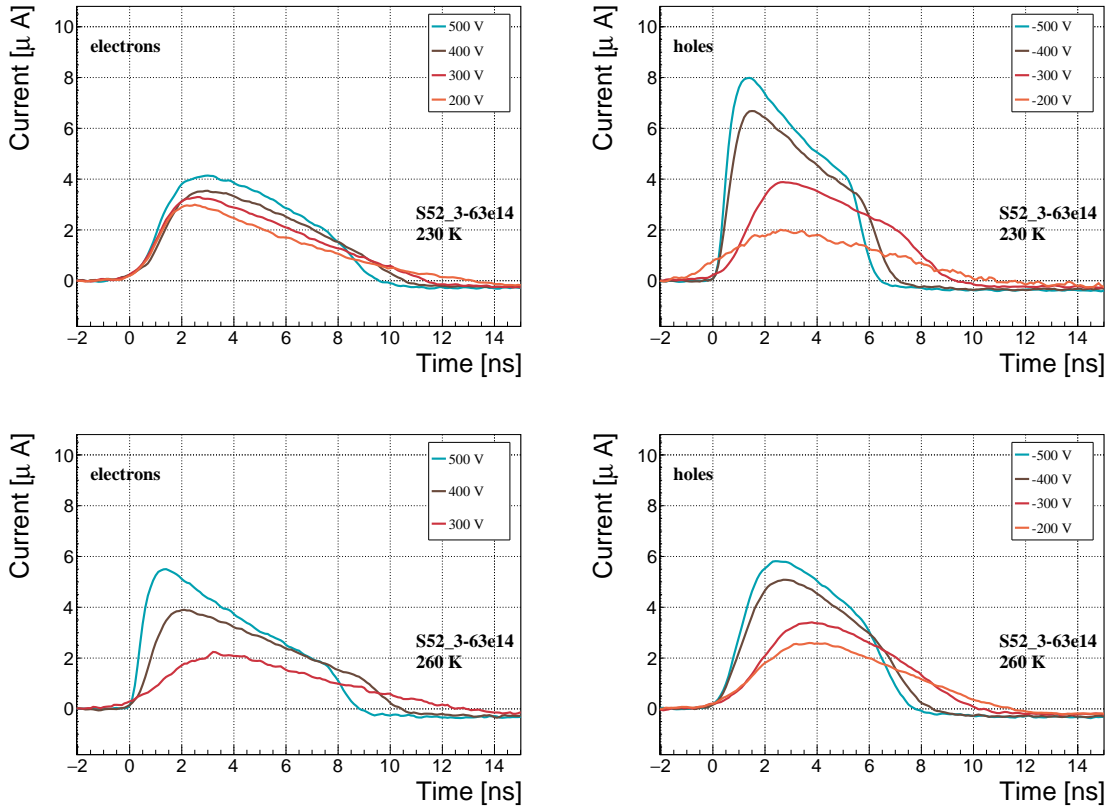


Figure 1.15: Varied bias voltage at a fixed temperature for an irradiated sample.

492     3. Reduce the measurement time at every bias voltage setting.

493     Unfortunately, options (1) and (2) are very time consuming and would increase the overall  
 494     experiment time to over one day. The third option would worsen the resulting averaged  
 495     pulses. In the end an alternative option has been chosen: alternating the starting bias  
 496     voltage and the sequence at every temperature point. With this option, a meaningful  
 497     systematic error in analysing the pulse shapes can be attained.

498     Figure 1.16 shows the irradiated S52 and S79 as well as the non-irradiated S37 for  
 499     comparison, all at a bias voltage of ±500 V and at several temperature points between 4 K  
 500     and 295 K. It is evident that the radiation damage affects the shape of the pulses across all  
 501     temperatures.

## 502     **Collected charge as a function of temperature**

503     The collected charge as a function of temperature for electrons and holes is plotted in  
 504     figures 1.17 and 1.18, respectively. In the framework of this thesis the focus is on the  
 505     effect in the irradiated devices. The new contribution are the data points for the irradiated  
 506     samples. The focus is on the temperature range between 4–75 K and 150–295 K whereby  
 507     the effect of the re-excitation of bound electrons and holes is not prevailing. The values

#### 1.4. TEMPERATURE LIMITATIONS

---

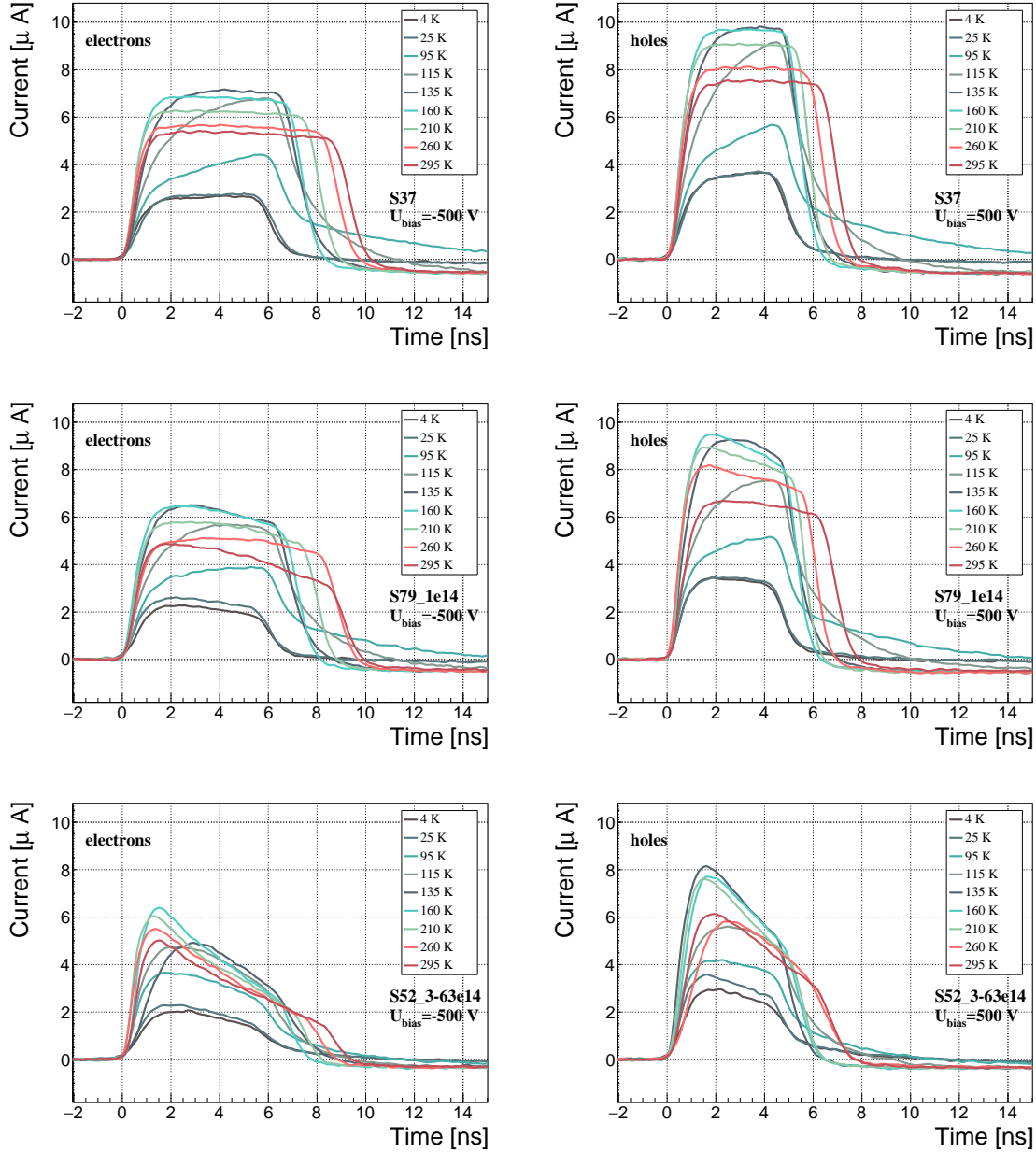


Figure 1.16: After irradiation: several data points between 4 K and 295 K at a bias voltage of  $\pm 500$  V.

for all samples are fairly stable in the range between 4 K and 75 K and between 150 K and 295 K. However, in the values for the irradiated S52 some excursions can be observed. This is due to the sequence of the measurement steps, which results in a hysteresis effect explained in the preceding text.

The collected charge drops significantly from 150 K down to 75 K. In the non-irradiated samples the values in the lower temperature range are approximately 30 % of those in the high range. For the irradiated samples this difference is lower: 35 % for S79 and 50 % for

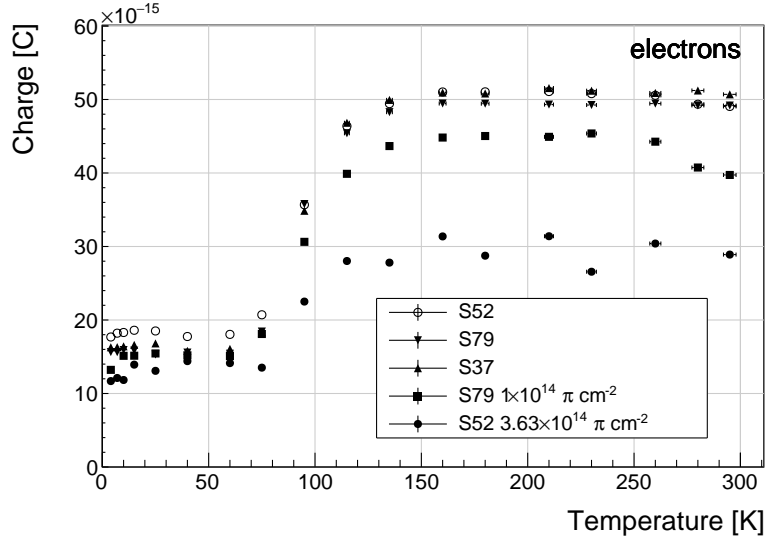


Figure 1.17: Collected charge for electrons as a function of temperature.

515 S52.

516 An interesting detail in figure 1.17 is that the ratio between the values for non-irradiated  
517 samples and their irradiated counterparts at the lower temperature range is different than  
518 at the higher range. In other words, the charge loss due to irradiation damage is lower for  
519 temperatures between 4 K and 75 K than for temperatures between 150 K and 295 K. The  
520 irradiated S52 collects 78 % of the initial charge in the low temperature range, but only  
521 59 % of the initial charge for the high range. The values for S79 for these two temperature  
522 ranges are 100 % and 90 %, meaning that the drop in charge collection efficiency after  
523 irradiation to  $1 \times 10^{14} \pi \text{ cm}^{-2}$  is negligible for temperatures below 75 K.

524 **Charge trapping**

525 A decaying exponential function from equation ?? has been fitted to the decaying top of the  
526 averaged pulses at a bias voltages of  $\pm 400 \text{ V}$  and  $\pm 500 \text{ V}$  across all temperatures excluding  
527 the transitional range between 75 K and 150 K. The resulting decay time constants  $\tau$  for  
528 an individual temperature point are not equal, which stems from the fact that the pulses  
529 change with time due to “polarisation”. This counts as a systematic error. Therefore the  
530 fitted  $\tau$  for  $\pm 400 \text{ V}$  and  $\pm 500 \text{ V}$  are averaged into one value representing the measurement  
531 at that temperature point. Figure 1.19 shows the fitted  $\tau$  for the five samples between 4 K  
532 and 295 K. In principle the time constants should be infinite for an ideal and non-irradiated  
533 sample. Here a slightly tilted top of the pulse due to space-charge is already successfully  
534 fitted with an exponential function (a pitfall in the automatic analysis), resulting in a  $\tau$   
535 of the order of  $(200 \pm 20) \times 10^{-9} \text{ s}$ . Consequently the fitting method is not adequate for  
536 non-irradiated samples.

537 For the irradiated samples the fit becomes increasingly more meaningful. As seen in fig-

## 1.4. TEMPERATURE LIMITATIONS

---

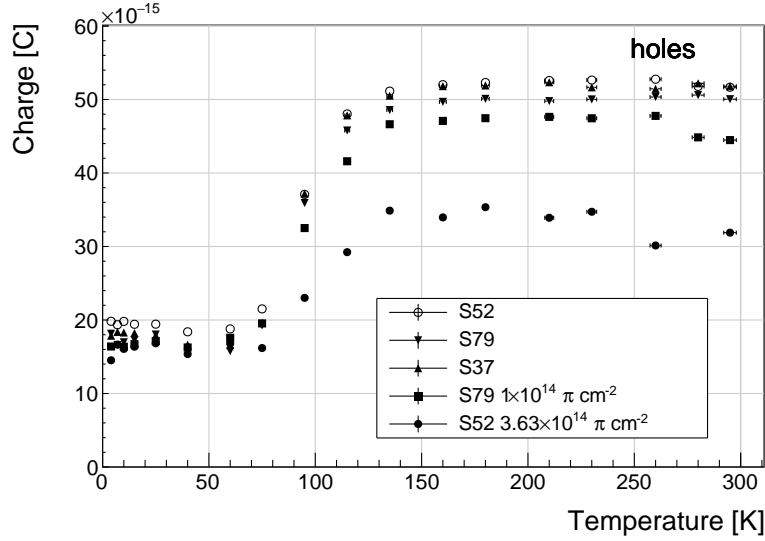


Figure 1.18: Collected charge for holes as a function of temperature.

538 ure 1.19, the fitted values of the irradiated samples are fairly stable across all temperatures.  
 539 There is a slight increase in the decay time constant of the S52 from  $(6.0 \pm 0.5) \times 10^{-9}$  s  
 540 above 150 K to  $(8.5 \pm 0.9) \times 10^{-9}$  s below 75 K. On the other hand, this step is not observable  
 541 in the S79 data. With only one sample exhibiting this behaviour, the effect is not significant  
 542 enough. Judging by the data acquired, the samples would need to be irradiated to doses  
 543 above  $1 \times 10^{14} \pi \text{ cm}^{-2}$  to quantify this effect in detail. So far this effect is not regarded  
 544 as significant for the scope of this thesis. Building on this assumption, the conclusion is  
 545 that the signal decay time constant for irradiated sCVD diamond is constant across the  
 546 temperature range between 4 K and 295 K, excluding the transitional range between 75 K  
 547 and 150 K where it cannot be quantified properly.

548 Considering the discussion above, all the values can be averaged into one decay constant.  
 549 Figure 1.20 shows these values for all samples as a function of the received  $\pi_{300}$  MeV radiation  
 550 dose. To estimate the charge carrier lifetime with respect to the radiation dose received, a  
 551 similar model is used than that in section 1.5. This model states that the charge carrier  
 552 lifetime is linearly decreasing with increasing radiation dose:

$$\frac{1}{\tau} = \frac{1}{\tau_0} + \kappa_\tau \cdot \Phi \quad (1.8)$$

$$\tau = \frac{\tau_0}{\kappa_\tau \tau_0 \Phi + 1} \quad (1.9)$$

553 where  $\tau_0$  is the lifetime for a non-irradiated sample (real lifetime, therefore of the order of  
 554 400 ns),  $\tau$  is the lifetime of an irradiated sample,  $\Phi$  is the received radiation dose and  $\kappa_\tau$  the  
 555 lifetime degradation factor. For these data the fitted factor is equal to  $\kappa_\tau = (3.5 \pm 0.8) \times$   
 556  $10^{-16} \text{ s cm}^2 \pi_{300}^{-1} \text{ MeV}$ . Using this factor, the steepness of the decay in the pulse shape as a  
 557 function radiation dose can be estimated. This is highly useful information when designing  
 558 a system where the current pulse shape is an important factor.

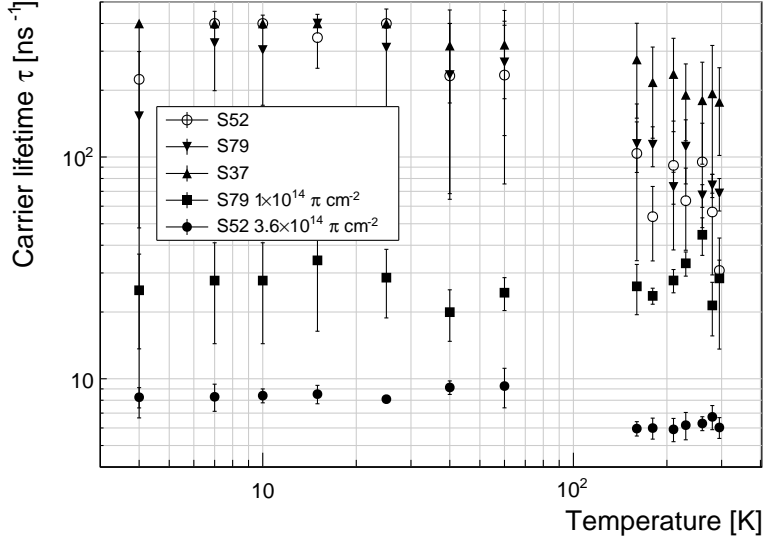


Figure 1.19: This figure shows the charge carrier lifetime as a function of temperature. The data points between 75 K and 150 K are omitted. The fit function only works well on signals with a well pronounced decaying top.

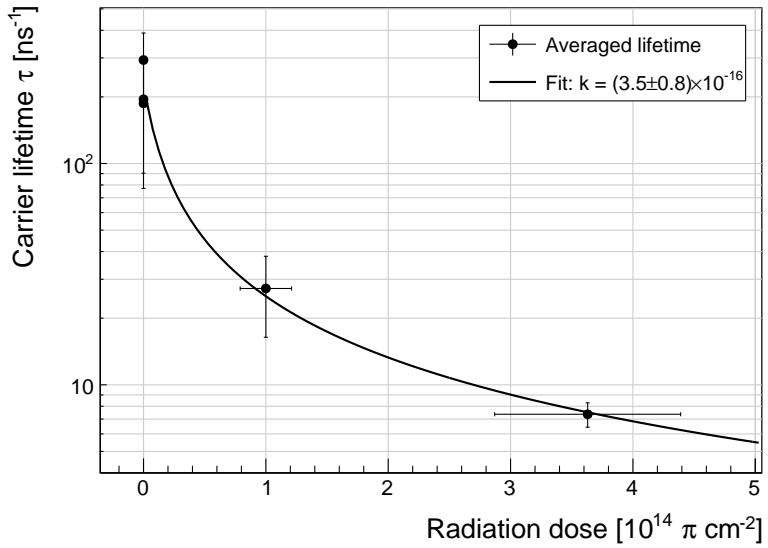


Figure 1.20: This figure shows the carrier lifetime averaged over all temperatures and plotted as a function of the  $\pi$  irradiation dose.

## 560 1.5 Conclusion

561 This chapter gives an overview of the capabilities and limitations of diamond as a particle  
562 detector. Two effects on diamond are studied – radiation and temperature.

563 Two sCVD diamond detectors were irradiated with 300 MeV pions. They were tested  
564 alongside a non-irradiated sample to observe the changes in the ability to detect  $\alpha$ ,  $\beta$  and

## 1.5. CONCLUSION

---

565  $\gamma$  radiation. Their charge collection efficiency was measured in a test beam facility. The  
566 results were compared to the results from the RD42 collaboration and a DPA model. A  
567 radiation damage factor  $k_\lambda = (4.4 \pm 1.2) \times 10^{-18} \mu\text{m}^{-1} \text{cm}^{-2}$  was obtained for  $\pi_{300} \text{ MeV}$   
568 particles. The data point was not in agreement with the data provided by RD42 nor with  
569 the model. However, the irradiation process and the low number of tested samples hold a  
570 relatively high statistical uncertainty. In addition, there was no diamond surface treatment  
571 done in between the measurements, as is the case in the study conducted by RD42. The  
572 results obtained in the course of these measurements are going to be fed into the existing  
573 pool of data in the RD42 collaboration.

574 The next step was to test the long-term capabilities for  $\alpha$  detection. The shape of the  
575 ionisation profile was investigated to determine the behaviour of the charge carriers in the  
576 irradiated diamond. An exponential decay was observed in the pulses of irradiated samples,  
577 proving that there are charge traps in the bulk that were created during irradiation. Then  
578 a long-term stability test was carried out. The results show that the irradiated diamond  
579 detectors do not provide a stable and reliable long-term measurement of  $\alpha$  particles. This  
580 might be due to a space-charge build-up in the bulk, which changes the electric field,  
581 affecting the charge carriers. A procedure to improve the pulse shape using  $\beta$  and  $\gamma$  radiation  
582 was proposed.

583 Finally, the diamond sensors were cooled down to temperatures between 4 K and 295 K.  
584 Their response to  $\alpha$  particles was observed. The results of the non-irradiated and irradiated  
585 samples were compared. The effect of reduction for the number of drifting charges due to  
586 exciton recombination was observed in both sets of data. The second set had a superimposed  
587 effect of charge trapping during the drift, which was represented by an exponential decay  
588 in the signal. The decay time constant did not change with temperature. Therefore all  
589 temperature points for individual samples were averaged and the decay time constants were  
590 plotted against the received radiation dose. A lifetime degradation factor  $\kappa_\tau = (3.5 \pm 0.8) \times$   
591  $10^{-16} \text{ s cm}^2 \pi_{300}^{-1} \text{ MeV}$  for non-primed diamonds was defined.